Error Vector Magnitude Optimization for OFDM Systems With a Deterministic Peak-to-Average Power Ratio Constraint

Qijia Liu, *Student Member, IEEE*, Robert J. Baxley, *Member, IEEE*, Xiaoli Ma, *Senior Member, IEEE*, and G. Tong Zhou, *Senior Member, IEEE*

***Abstract*—Orthogonal frequency division multiplexing (OFDM) has been adopted by several wireless transmission standards. A major disadvantage of OFDM is the large dynamic range of its time-domain waveforms, making OFDM vulnerable to nonlinearities (including clipping effects) of the power amplifier (PA) and causing the PA to yield low efficiency on the RF to dc power conversion. A commonly used metric to characterize a signal's dynamic range is the peak-to-average power ratio (PAR). To suppress the nonlinear effects, one may want to reduce the signal PAR. However, this results in the increase of error vector magnitude (EVM), and may violate the spectral mask. In this paper, we formulate the problem as an EVM optimization task subject to a deterministic PAR constraint and a spectral mask constraint. A low-complexity customized interior-point algorithm is developed to solve the optimization problem. We also discuss extensions of the optimization framework, whereby we optimize the parameters with respect to two metrics on signal-to-noise-and-distortion ratio (SNDR) and mutual information, respectively.**

***Index Terms*—Error vector magnitude (EVM), orthogonal frequency division multiplexing (OFDM), peak-to-average power ratio (PAR), power efficiency.**

I. Introduction

DUE to its high spectral efficiency and robustness against frequency-selective fading channels, the orthogonal frequency division multiplexing (OFDM) technique has been adopted by many wireless communication standards [1]–[3]. However, one of the primary disadvantages of OFDM is that time-domain OFDM waveforms exhibit large peak-to-average power ratios (PARs) [4]. In order to avoid severe nonlinear distortions both in-band and out-of-band, power amplifiers (PAs) are often operated with a large input back-off (IBO), resulting in poor efficiency on the RF to dc power conversion [5].

Any PAR reduction method has to modify the signal waveform in some fashion. With a distortionless PAR reduction technique, some sort of reverse operation is done at the receiver requiring receiver-side modifications. In this paper, we are interested in PAR reduction techniques that make changes to the transmitter only without receiver-side cooperation. This excludes distortionless techniques such as [6]–[8], and forces us to pursue distortion-based techniques only. The key is to carefully manage the distortions so we stay within the limits as specified in the communication standards.

Distortion-based PAR reduction algorithms have been investigated in [4], [5], and [9]–[17]. Some operate by constraining the distortion energy on data subcarriers [11]–[13]; some by projecting the distortion energy onto "free" or "reserved" subcarriers [5], [14], [15]. In the recent literature [16], [17], PAR reduction has been cast as a convex optimization problem where the symbol-wise PAR is minimized subject to a symbol-wise error vector magnitude (EVM) constraint. By exploiting the fast Fourier transform (FFT) structure of OFDM, an interior-point method (IPM) can be devised to solve the convex optimization problem efficiently thus providing good PAR reduction performance with relatively low complexity.

In communication standards, EVM is widely adopted to quantify the amount of in-band distortion that occurs at the transmitter, and directly affects performance like bit error rate (BER) at the receiver. EVM can be caused by any number of non-ideal components in the transmission chain, including the PA, the digital-to-analog converter (DAC), the mixer, etc. A distortion-based PAR reduction algorithm increases the EVM as well. We assume that there is sufficient EVM "headroom" left from the analog devices to allow for a distortion-based PAR reduction algorithm.

In [16] and [17], symbol-wise EVM constraints are used in the symbol-wise PAR minimization algorithm. In communication standards, however, a root mean-square (RMS) EVM constraint is typically given, which means that the symbol-wise EVM can fluctuate from symbol to symbol and does not have to be as tightly constrained as in [16] and [17]. Our strategy here is to take advantage of this degree of freedom in the symbol-wise EVM to boost the PAR reduction performance.

In a block communication system, minimizing the symbol-wise PAR as pursued in the existing PAR reduction literature does not automatically yield power efficiency

Manuscript received April 29, 2008; revised March 23, 2009. Current version published May 15, 2009. This work was supported in part by the U. S. Army Research Laboratory under the Collaborative Technology Alliance Program, Cooperative Agreement DAAD19-01-2-0011 and in part by the National Science Foundation Graduate Research Fellowship Program. Some results of this paper were presented at the IEEE Conference on Information Sciences and Systems, Princeton, NJ, March 19–21, 2008. The associate editor coordinating the review of this manuscript and approving it for publication was Prof. Marc Moonen.

Q. Liu, X. Ma, and G. T. Zhou are with the School of Electrical and Computer Engineering, Georgia Institute of Technology, Atlanta, GA 30332-0250 USA (e-mail: qjliu@ece.gatech.edu; xiaoli@ece.gatech.edu; gtz@ece.gatech.edu).

R. J. Baxley is with the Information Technology and Telecommunications Lab (ITTL), Georgia Tech Research Institute, Atlanta, GA 30318 USA (e-mail: bob.baxley@gtri.gatech.edu).

Color versions of one or more of the figures in this paper are available online at http://ieeexplore.ieee.org.

Digital Object Identifier 10.1109/JSTSP.2009.2020239

improvements, unless one implements adaptive biasing or adaptive scaling [18] to boost the average transmit power of PAR-reduced symbols. The method we propose here does not require block-to-block adaptive biasing or adaptive scaling because we can predetermine a PAR threshold based on the spectral mask and RMS EVM goals. Note that we are interested in a fixed PAR threshold for all signal blocks rather than optimum but variable PAR values from block to block. Once the PAR threshold is judiciously chosen, the PA's size, bias, and/or IBO can be determined so that the PA's linear dynamic range corresponds to the PAR threshold chosen. Since the PAR of the modified OFDM signal never exceeds the prescribed PAR threshold, PA clipping and the associated EVM and spectral distortion increases are prevented. We will develop a low complexity interior-point method to solve the proposed EVM minimization problem. We also offer insight regarding optimal tradeoffs between in-band distortion and power efficiency in order to comply with the standard's requirements on EVM and spectral mask.

Our proposed method differs from existing approaches in the following ways. 1) We target the RMS EVM rather than the symbol-wise EVM. This is not only standard-oriented, but also results in better PAR reduction performance. When the RMS EVM constraint is used, certain large PAR symbols can be allocated greater symbol-wise EVM budget to permit significant PAR reduction. If an OFDM symbol has a small PAR value to start with, very little symbol-wise EVM allowance may be needed in order to reach the PAR threshold. It is easier to achieve a RMS EVM goal than to achieve a symbol-wise EVM goal of the same magnitude. Therefore, when the RMS EVM metric is used, there is more room for the PAR algorithm to do its work. 2) A deterministic PAR constraint is used. Assuming a soft-limiter PA, peak-power limited symbols achieved with the proposed algorithm avoid the possibility of in-band distortion, out-of-band spectral regrowth and average power reduction, which are caused by PA clipping.

The organization of the rest of the paper is as follows. The OFDM system model and the PAR problem are outlined in Section II. We formulate and discuss the PAR constrained optimization framework in Section III. Numerical results are shown in Section IV and conclusions are drawn in Section V. Details of the customized interior-point method and a signal-to-noise-and-distortion ratio (SNDR) approximation are given in the Appendices.

II. System Model

Let $\mathbf{X} = [X_{-N/2}, \cdots, X_{N/2-1}]^T$ denote a frequency-domain OFDM symbol with N subcarriers; ^{T} stands for transpose. By zero-padding $\mathbf{X}$ with $(L-1)N$ zeros, we obtain

$$\mathbf{X}^{(L)} = \left[X_0^{(L)}, \cdots, X_{LN-1}^{(L)}\right]^T = \left[X_0, \cdots, X_{\frac{N}{2}-1}, 0, \cdots, 0, X_{-\frac{N}{2}}, \cdots, X_{-1}\right]^T. \quad (1)$$

An inverse FFT (IFFT) operation is performed to generate the time-domain signal, i.e.,

$$x^{(L)}[n] = \mathrm{IFFT}\left(\mathbf{X}^{(L)}\right)[n] = \frac{1}{\sqrt{LN}} \sum_{k=0}^{LN-1} X_k^{(L)} e^{\frac{j2\pi kn}{LN}}. \quad (2)$$

For notational simplicity, let us drop $^{(L)}$ from now on and denote the time-domain waveform as $\mathbf{x} = [x[0], \cdots, x[LN-1]]^T$ with ensemble mean power $\sigma_x^2 \triangleq \sigma_{x[n]}^2 = E[|x[n]|^2]$, which is equal to the infinite-time average power because $\mathbf{x}$ is ergodic. PAR of the time-domain waveform is defined as

$$\mathrm{PAR}(\mathbf{x}) = \max_{n \in \{0, \cdots, LN-1\}} \frac{|x[n]|^2}{\sigma_x^2} \quad (3)$$

which is unchanged after the cyclic extension.

Input back-off (IBO) is defined as the ratio between the maximum PA input power before reaching saturation and the average power of the input signal. IBO needs to be made large enough to accommodate the (occasional) large peaks of the input signal [18], [19]. Large IBO however, diminishes the transmission power efficiency.

According to the Central Limit Theorem, the time-domain waveform $\mathbf{x}$ exhibits an approximate complex Gaussian distribution when N is reasonably large. As a result, $\mathbf{x}$ can have certain large PAR values with nonzero probabilities. When these large PAR values exceed the IBO, clipping will occur thus generating EVM and spectral broadening (spectral regrowth) that may exceed the distortion limits imposed by the standards or that are difficult to predict and control.

Denote $x(t)$ and $y(t)$ as the input and output signals of the PA respectively. In this paper, a PA with an ideal soft limiter characteristic is assumed, meaning that

$$|y(t)| = \begin{cases} \mathcal{G} \cdot |x(t)|, & |x(t)| \le \mu_{\mathrm{in}} \\ \mathcal{G} \cdot \mu_{\mathrm{in}}, & |x(t)| > \mu_{\mathrm{in}} \end{cases} \quad (4)$$

$$\angle y(t) = \angle x(t) \quad (5)$$

where μ_{in} stands for the saturation level of the PA input and $\mathcal{G}$ is the PA gain in the linear region [5, ch. 3]. Although the piecewise linear characteristic is a simplifying assumption, it is feasible when PA linearization (for example, via predistortion) is implemented [20], [21].

For the ideal soft limiter PA, the IBO can be expressed as

$$\mathrm{IBO} = \frac{\mu_{\mathrm{in}}^2}{\mathcal{B}^2 \sigma_x^2} \quad (6)$$

where $\mathcal{B}$ is the multiplier used for achieving the given IBO. Because the dc power of a class-A PA is twice its peak output power, i.e., $P_{\mathrm{dc}} = 2\mathcal{G}^2\mu_{\mathrm{in}}^2$, the power efficiency is [22]

$$\rho = \frac{\mathcal{G}^2\mathcal{B}^2\sigma_x^2}{P_{\mathrm{dc}}} = \frac{1}{2 \cdot \mathrm{IBO}}. \quad (7)$$

Given the same PA, the larger the IBO, the lower the power efficiency. If the PAR has nonzero probability of exceeding the IBO, the signal still will be clipped. Thus, the standard's requirements like EVM may be violated. Therefore, it is desirable

to have an algorithm which guarantees that the PAR of the modified OFDM signal will never exceed a given threshold so that no PA clipping may be encountered. This motivates the research in this paper.

According to the standards [2], [3], the OFDM subcarriers are usually categorized into three non-overlapping sets: pilot subcarriers, free subcarriers and data subcarriers, denoted by sets of indices $\mathcal{K}_p$, $\mathcal{K}_f$, and $\mathcal{K}_d$, respectively. They have the cardinalities $|\mathcal{K}_p| = p$, $|\mathcal{K}_f| = f$, and $|\mathcal{K}_d| = d$ so that $p + f + d = N$.

The signal transmitted over the pilot subcarriers is known *a priori* to the receivers, denoted as $X_k = \mathcal{P}_k$ $(k \in \mathcal{K}_p)$. For instance, the pilot signals are defined as $\mathcal{P}_k \in \{\pm 1\}$ $(k \in \mathcal{K}_p)$ in the IEEE 802.11a standard [2]. In order not to interfere with the channel estimation, transmitters are not allowed to modify these pilot signals. Denote $\mathbf{X}^\dagger$ as the modified symbol whose time-domain counterpart $\mathbf{x}^\dagger$ has a lower PAR than the original waveform $\mathbf{x}$. Thus, we have $X_k^\dagger = X_k$ $(k \in \mathcal{K}_p)$.

On the free subcarriers, any complex value $X_k^\dagger \in \mathcal{C}$ $(k \in \mathcal{K}_f)$ subject to the spectral mask constraint as specified in the standards can be transmitted, i.e.,

$$E\left[\left|X_k^\dagger\right|^2\right] \le \mathcal{M}_k \cdot P_0, \quad k \in \mathcal{K}_f \tag{8}$$

where $\mathcal{M}_k$ represents the relative spectral mask constraints and $P_0 = E[|X_k|^2]$ $(k \in \mathcal{K}_d)$ is the average power of the data subcarriers or the constellation itself [2]. Referring to the definition of σ_x^2, one can show that $dP_0 + \sum_{k \in \mathcal{K}_p} |\mathcal{P}_k|^2 = LN\sigma_x^2$.

On the data subcarriers, the information bits are mapped into an ideal constellation Ω of the modulation schemes specified in the standards, namely $X_k \in \Omega$ $(k \in \mathcal{K}_d)$. However, a certain amount of in-band distortion is allowed. Such in-band distortion may arise as the result of the PAR reduction. Firstly, the symbol-wise EVM is defined as

$$\epsilon(\mathbf{X}, \mathbf{X}^\dagger) = \sqrt{\frac{\frac{1}{d}\sum_{k \in \mathcal{K}_d}\left|X_k - X_k^\dagger\right|^2}{P_0}}. \tag{9}$$

In communication standards, the in-band distortion is constrained in terms of the RMS EVM constraint. The RMS EVM value must be less than or equal to the threshold ε which is set forth in the standards, i.e.,

$$\text{RMS EVM} = \sqrt{E\left[\epsilon(\mathbf{X}, \mathbf{X}^\dagger)^2\right]} \le \varepsilon. \tag{10}$$

III. EVM Optimization Framework

In this paper, we adopt a deterministic (as opposed to probabilistic) PAR constraint

$$\text{PAR} \le \gamma. \tag{11}$$

When $\text{IBO} = \gamma$, the modified signal $\mathbf{x}^\dagger$ will not experience PA clipping. On the other hand, one can first determine the IBO necessary to ensure a certain level of linearity and power efficiency from the PA and then set $\gamma = \text{IBO}$. The target IBO should lie within the feasibility region as discussed later in this paper. A smaller γ leads to higher power efficiency but also larger RMS EVM and higher computational cost. The lowest possible γ can be calculated based on the RMS EVM and spectral mask constraints. For a given RMS EVM threshold and spectral mask, our algorithm finds the lowest PAR threshold (or the highest power efficiency), that any distortion-based PAR reduction method should obey.

Next, we formulate the EVM optimization algorithm that minimizes the symbol-wise EVM while simultaneously satisfying the deterministic PAR constraint in (11) and the spectral mask constraint in (8)

$$\begin{aligned}
\underset{\mathbf{X}^\dagger}{\text{minimize}} \quad & e && (12)\\
\text{subject to} \quad & \sqrt{dP_0}\cdot\epsilon(\mathbf{X}, \mathbf{X}^\dagger) \le e && (13)\\
& X_k^\dagger = X_k,\ k \in \mathcal{K}_p && (14)\\
& \left|X_k^\dagger\right|^2 \le \mathcal{M}_k \cdot P_0,\ k \in \mathcal{K}_f && (15)\\
& \sum_{k \in \mathcal{K}_d} \Re\left(X_k^*\left(X_k^\dagger - X_k\right)\right) \ge -\frac{e^2}{2} && (16)\\
& \mathbf{x}^\dagger = \text{IFFT}_L(\mathbf{X}^\dagger) && (17)\\
& \left|x^\dagger[n]\right| \le \sqrt{\gamma}\sigma_x,\ n = 0, \cdots, LN-1 && (18)
\end{aligned}$$

where $\Re(x)$ denotes the real part of x. In particular, (12) and (13) set the symbol-wise EVM, $\epsilon(\mathbf{X}, \mathbf{X}^\dagger)$, as the objective for minimization. Equation (14) keeps the pilot subcarriers unchanged. Equation (15) constrains the instantaneous power of the free subcarriers to satisfy the spectral mask requirement. Although (15) provides a stricter constraint than (8), it is easier to solve symbol-wise. Additionally, since directly constraining the PAR leads to a complicated nonconvex problem, we follow the derivation in [16] and separately restrict the peak power as in (18), and the average power on data subcarriers according to (16). Equation (16) is a convex inequality constraint and is equivalent to

$$\sum_{k \in \mathcal{K}_d}\left|X_k^\dagger\right|^2 \ge \sum_{k \in \mathcal{K}_d}|X_k|^2 \tag{19}$$

when the constraint of (13) is tight (i.e., $\sqrt{dP_0}\epsilon(\mathbf{X}, \mathbf{X}^\dagger) = e$), which always holds in optimality. Later, we will show that (16) and (18) guarantee that the PAR of the optimized signal $\mathbf{x}^\dagger$ will never exceed the threshold γ.

This EVM optimization framework is a convex optimization problem and can be solved by the customized interior-point method (IPM). The details of IPM are given in Appendix A. In the following, we list some properties of the proposed EVM optimization algorithm.

A. Properties of the EVM-Optimized Signals

1) Peak Power Limited for the PA Input Signal: After setting the IBO, the PA input signal becomes $\mathcal{B}x^\dagger[n]$ whose peak magnitude is limited according to (18) as

$$\max\left|\mathcal{B}x^\dagger[n]\right| \le \frac{1}{\sigma_x}\sqrt{\frac{\mu_{\text{in}}^2}{\text{IBO}}}\cdot\sqrt{\gamma}\sigma_x = \sqrt{\frac{\gamma}{\text{IBO}}}\cdot\mu_{\text{in}}. \tag{20}$$

By choosing $\text{IBO} \ge \gamma$ in (20), the peak magnitude is always less than or equal to μ_{in}, eliminating the possibility of PA saturation.

2) Average Power: From (19), it is straightforward to infer that for the data subcarriers

$$E\left[\sum_{k\in\mathcal{K}_d}\left|X_k^\dagger\right|^2\right]\geq E\left[\sum_{k\in\mathcal{K}_d}|X_k|^2\right]=dP_0. \tag{21}$$

Equation (21) says that with the proposed algorithm, the average transmitted power on the data subcarriers is increased. Also, because the signals on free subcarriers of the original symbol $\mathbf{X}$ are zero, we have

$$E\left[\sum_{k\in\mathcal{K}_f}\left|X_k^\dagger\right|^2\right]\geq E\left[\sum_{k\in\mathcal{K}_f}|X_k|^2\right]=0. \tag{22}$$

Recall that the pilot subcarriers are unchanged and $\mathcal{K}_d\cup\mathcal{K}_f\cup\mathcal{K}_p=\{-N/2,\cdots,N/2-1\}$, we have [cf. (21) and (22)]

$$E\left[\sum_{k=-N/2}^{N/2-1}\left|X_k^\dagger\right|^2\right]\geq E\left[\sum_{k=-N/2}^{N/2-1}|X_k|^2\right]. \tag{23}$$

By Parseval's theorem, the average power of the time-domain EVM-optimized signal has

$$\sigma_{x^\dagger}^2\geq\sigma_x^2. \tag{24}$$

Because no clipping occurs at the PA, the average power of the transmitted signal is

$$\mathcal{G}^2\mathcal{B}^2\sigma_{x^\dagger}^2. \tag{25}$$

3) Deterministic PAR Constraint: The PAR of the optimized signal $\mathbf{x}^\dagger$ is upper bounded by the deterministic threshold γ

$$\mathrm{PAR}(\mathbf{x}^\dagger)=\max_{n\in\{0,\cdots,LN-1\}}\frac{\left|x^\dagger[n]\right|^2}{\sigma_{x^\dagger}^2}\leq\gamma. \tag{26}$$

4) Spectral Mask Constraint: Because of (21), the EVM-optimized signal $\mathbf{X}^\dagger$ strictly satisfies the relative spectral mask constraint

$$E\left[\left|X_k^\dagger\right|^2\right]\leq\mathcal{M}_k\cdot P_0\leq\mathcal{M}_k\cdot P_0^\dagger,\ k\in\mathcal{K}_f \tag{27}$$

where $P_0^\dagger=(1/d)E[\sum_{k\in\mathcal{K}_d}|X_k^\dagger|^2]$ is the average power on the data subcarriers of $\mathbf{X}^\dagger$.

5) SNDR of Peak-Power-Limited Transmitters: The signal-to-noise-and-distortion ratio (SNDR) is another metric to characterize nonlinear distortions [23]. The EVM-optimized signal $\mathbf{x}^\dagger$ (or $\mathbf{X}^\dagger$) is a highly nonlinear function of the original OFDM signal $\mathbf{x}$ (or $\mathbf{X}$). According to Bussgang's theorem [24], the data subcarriers of $\mathbf{X}^\dagger$ can be decomposed as

$$X_k^\dagger=\alpha X_k+\omega_k,\ \forall k\in\mathcal{K}_d \tag{28}$$

where $\omega_k(k\in\mathcal{K}_d)$ denotes the distortion noise with variance $\sigma_\omega^2=E[|X_k^\dagger|^2]-|\alpha|^2E[|X_k|^2]$. α is a constant chosen so that ω_k is uncorrelated with X_k, i.e., $\alpha=E[X_k^*X_k^\dagger]/E[|X_k|^2]$ and thus $E[X_k^*\omega_k]=0$ where the expectations are evaluated over X_k and $X_k^\dagger$ on $k\in\mathcal{K}_d$ and all OFDM symbols. The SNDR of the kth data subcarrier of the output signal is thus defined as [11]

$$\mathrm{SNDR}_k=\frac{|h_k|^2\left(\mathcal{G}\mathcal{B}|\alpha|\right)^2E\left[|X_k|^2\right]}{|h_k|^2(\mathcal{G}\mathcal{B})^2\sigma_\omega^2+\sigma_k^2},\ k\in\mathcal{K}_d \tag{29}$$

where h_k is the frequency-domain channel response and σ_k^2 is the channel noise power of the kth subcarrier. It can be approximately expressed as a function of the RMS EVM and γ as follows:

$$\mathrm{SNDR}_k\approx\frac{1-(\mathrm{RMS\ EVM})^2}{(\mathrm{RMS\ EVM})^2+\frac{2d\sigma_k^2}{rP|h_k|^2}\cdot\gamma},\ k\in\mathcal{K}_d \tag{30}$$

where $P=2LN(\mathcal{G}\mu_{\mathrm{in}})^2$ denotes the total power consumed by the peak-power-limited class-A PA for transmitting one OFDM symbol, and r is defined as the ratio between the power transmitted on the data subcarriers and the total power, i.e.,

$$r=\frac{E\left[\sum_{k\in\mathcal{K}_d}|X_k|^2\right]}{E\left[\sum_{k=-N/2}^{N/2-1}|X_k|^2\right]}=\frac{d\cdot P_0}{d\cdot P_0+\sum_{k\in\mathcal{K}_p}|\mathcal{P}_k|^2} \tag{31}$$

which is a constant and can be calculated according to the standards. The derivation of (30) is included in Appendix B.

B. Lower Bounds

The EVM optimization algorithm offers a way to numerically determine the fundamental tradeoff between in-band distortion and the power efficiency of peak-power-limited OFDM transmitters.

1) RMS EVM Lower Bounds: On one hand, the lower bound of RMS EVM values, denoted as $\varepsilon_{\mathrm{min}}$, can be determined for the given PAR threshold γ. The EVM optimization algorithm minimizes the symbol-wise EVM of each OFDM symbol. Therefore, the RMS EVM value found by the proposed algorithm is expected to be the minimum for the given deterministic PAR constraint.

2) PAR Lower Bounds: On the other hand, the minimum PAR threshold can be found for the RMS EVM constraints ε as specified in the standards.

In general, the higher the PAR threshold γ, the smaller the optimized symbol-wise EVM and RMS EVM tend to be. Therefore, we can determine, by offline Monte Carlo simulations, the lowest possible γ whose corresponding RMS EVM value meets the standard's requirement. The problem can be formulated as follows:

$$\text{minimize}\quad\gamma \tag{32}$$

$$\text{subject to}\quad\mathrm{RMS\ EVM}\leq\varepsilon \tag{33}$$

where RMS EVM is a function of γ and has to be numerically calculated. The resulting minimum PAR threshold, denoted as γ_{min}, gives the lower bound of the deterministic PAR threshold for the given RMS EVM threshold ε. In other words, no deterministic PAR constraint $\gamma<\gamma_{\mathrm{min}}$ is feasible for the given RMS EVM and spectral mask constraints in this system.

As shown in (7), the transmitter power efficiency can be maximized by minimizing the IBO. Also, $\mathrm{IBO} \geq \gamma$ is required. By setting $\mathrm{IBO} = \gamma_{\min}$, the maximum power efficiency, as a result, becomes

$$\rho_{\max} = \frac{1}{2\gamma_{\min}}. \tag{34}$$

C. SNDR Maximization

Because RMS EVM is a function of γ, the SNDR in (30) can be maximized over the PAR threshold γ for known channel information h_k and σ_k^2, i.e.,

$$\gamma^\star = \arg\max_{\gamma} \mathrm{SNDR}_k|_{h_k,\sigma_k^2}. \tag{35}$$

SNDR maximization is analogous to SNR maximization in non-peak-limited channels. Since SNDR is a measure of the ratio of signal power to uncorrelated noise/distortion power, it can substitute SNR in bit error rate (BER) or symbol error rate (SER) expressions to determine system performance. Thus, since all meaningful BER and SER expressions are monotonic in SNDR, it is important to determine the PAR threshold in (35) that maximizes SNDR.

In maximizing SNDR, the RMS EVM value that corresponds to $\gamma^\star$ may be different from (or even greater than) the constraint defined in those current communication standards, but we argue that this RMS EVM value and PAR threshold will introduce the optimal SNDR performance for the given peak-power-limited transmitters and channel. Intuitively, although in-band distortion is increased by using a smaller γ, the transmitted average power is increased such that the channel noise is equivalently suppressed. Using the γ-RMS EVM curves obtained *a priori* by (32) and (33), the optimal PAR threshold $\gamma^\star$ can be determined by the online calculation of (35) which is enabled by the SNDR approximation of (30). Then, the optimal tradeoff between in-band distortion and power efficiency can be reached by the EVM optimization algorithm.

D. Mutual Information Maximization

As was argued in the last subsection, SNDR is analogous to SNR in error rate expressions. Another pertinent optimization is mutual information maximization. Fortunately, a relationship between SNDR and capacity was derived in [23], which showed that because the distortion term w_k in (28) is approximately Gaussian distributed, the lower bound of the mutual information on each data subcarrier is $C_k \geq \log_2(1+\mathrm{SNDR}_k)$ bits/symbol ($\forall k \in \mathcal{K}_d$). Accordingly, when a flat channel is assumed such that $\mathrm{SNDR}_k = \mathrm{SNDR}$, the total system mutual information per symbol is lower bounded by

$$\sum_{k\in\mathcal{K}_d} C_k \geq d \cdot \log_2(1+\mathrm{SNDR}) = C \text{ bits/symbol}. \tag{36}$$

Unlike SNDR maximization, mutual information lower bound maximization involves a tradeoff in the number of data subcarriers, d. When more data subcarriers are used, the sum in (36) involves more terms leading to an apparent increase in the mutual information. However, these additional terms come at the expense of fewer free subcarriers (smaller f), which means less PAR reduction is possible and may cause an ultimately lower SNDR.

Finally, when using the EVM optimization algorithm of Section III, the pair (γ, f) should be selected so that the mutual information lower bound is maximized. It can be summarized as the following maximization problem:

$$\mathrm{maximize}_{\gamma,f} \quad C \tag{37}$$

where C is defined in (36). This lower bound is implicitly a function of the set of variables (γ, RMS EVM, f). With the help of offline calculated γ-RMS EVM curves for different f, the lower bound (36) can be evaluated and the maximization problem of (37) can be solved online with known channel information.

IV. Numerical Results

The simulation setup follows the IEEE 802.11a standard [2]. $L = 4$, $N = 64$ and the spectral mask as defined in the IEEE 802.11a standard was used [2]. Without loss of generality, the OFDM symbols were drawn from a normalized quadrature phase-shift keying (QPSK) constellation ($P_0 = 1$) for which the RMS EVM threshold is $\varepsilon = 0.1$. $p = 4$ subcarriers were used for transmitting the pilot signals at the indices of $\mathcal{K}_p = \{-21, -7, 7, 21\}$ with the binary values of $\{1, 1, 1, -1\}$, respectively.

A. EVM Optimization

In Section III-A, the EVM-optimized OFDM signal has been proved to have PAR values strictly less than or equal to the specified threshold γ. Fig. 1 shows the complimentary cumulative distribution function (CCDF) curves of the resulting PAR values for various PAR thresholds γ =3, 4, 5, 6, and 7 dB. The corresponding RMS EVM values of the PAR-reduced waveforms are also indicated. In this example, $f = 12$ free subcarriers were used as allocated in IEEE 802.11a [2]. We observe that these curves do not go beyond the $\eta = \gamma$ lines, thus confirming that the customized IPM does implement the intended deterministic PAR constraint.

In Fig. 2, the tradeoff curves between the RMS EVM values and the PAR threshold γ are shown for different numbers of free subcarriers (f = 0, 4, 8, 12). The γ-RMS EVM curves set the boundaries for system parameter designs. The feasibility regions only lie above these curves.

Fig. 2 indicates two kinds of lower bounds as discussed in Section III-B. First, for the assumed transmitter with the deterministic PAR constraint and spectral mask requirement, it gives the lower bound for the RMS EVM threshold $\varepsilon_{\min}$. For instance, Fig. 2 shows that the minimum RMS EVM threshold is $\varepsilon_{\min} = 0.035$ for $\gamma = 5$ dB and $f = 12$. It indicates that if $\mathrm{IBO} = 5$ dB is required for the system power efficiency, no distortion-based PAR reduction algorithm can have in-band distortion with RMS EVM less than 0.035.

Second, according to the RMS EVM threshold ε as specified in the standards, the minimum PAR threshold $\gamma_{\min}$ can be determined according to Fig. 2. For instance, since the RMS EVM threshold is $\varepsilon = 0.1$ for our simulation setup, only the curves

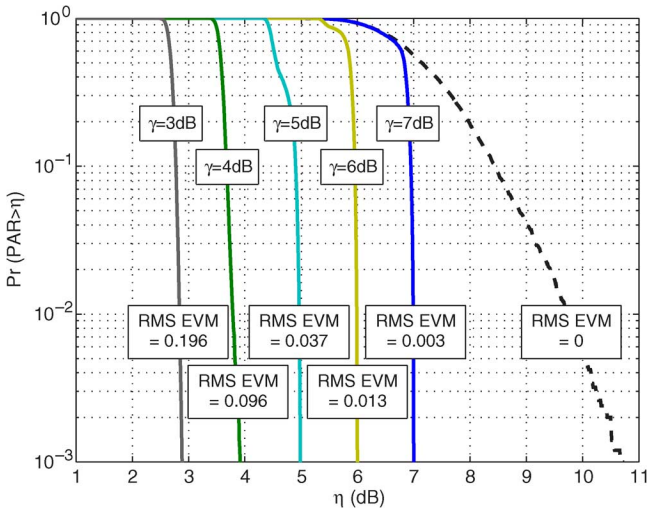

Fig. 1. CCDF curves of the PAR of the EVM-optimized signal $\mathbf{x}^{\dagger}$ for different PAR thresholds γ; the number of free subcarriers is $f = 12$. That of the PAR of the original OFDM signal is also shown.

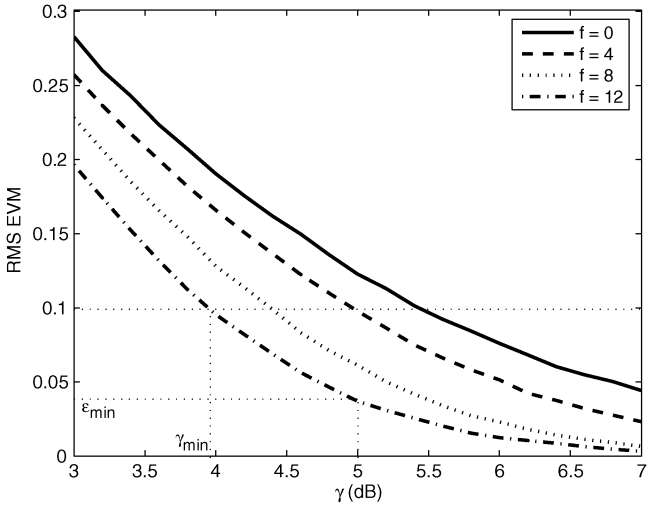

Fig. 2. RMS EVM of the EVM-optimized signal $\mathbf{x}^{\dagger}$ for different PAR threshold γ, when the number of free subcarriers f =0, 4, 8, 12.

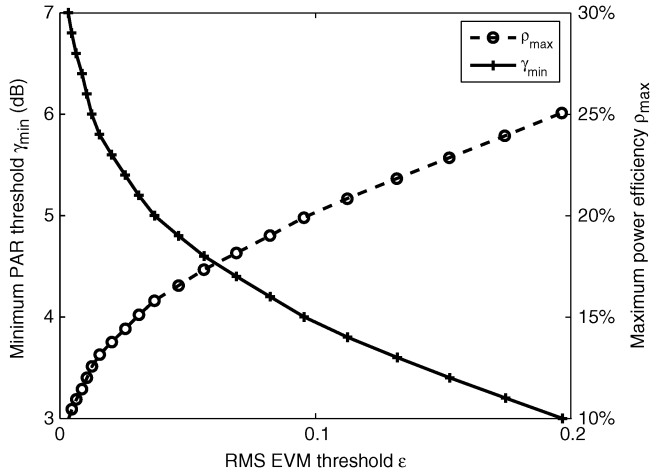

Fig. 3. Minimum PAR threshold $\gamma_{\min}$ and the maximum power efficiency $\rho_{\max}$ as the functions of RMS EVM threshold ε; the number of free subcarriers is $f = 12$.

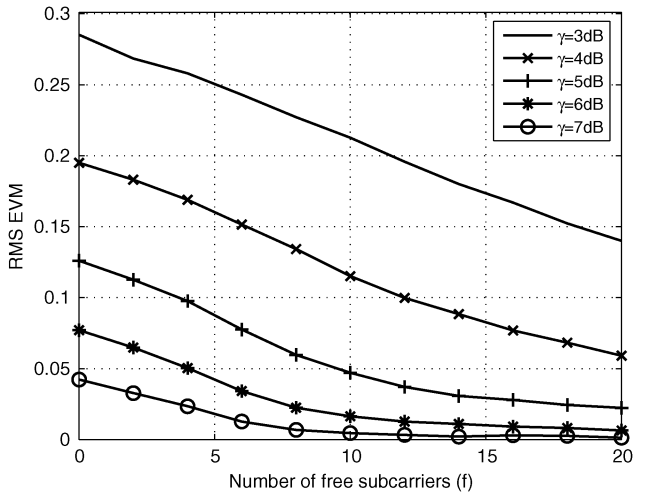

Fig. 4. RMS EVM of the EVM-optimized signal $\mathbf{x}^{\dagger}$ for different numbers of free subcarriers; the PAR threshold is γ =3, 4, 5, 6, 7 dB.

below the RMS EVM $= 0.1$ dotted line are allowed. As a result, the minimum PAR threshold is about $\gamma_{\min} = 3.95$ dB when $f = 12$ free subcarriers are to be employed. Any requirement for a PAR threshold lower than 3.95 dB is unrealistic if the RMS EVM is expected to be $\leq$0.1. When compared with the original OFDM signal, a PAR reduction of 6.6 dB was readily achieved at the 10^{-3} CCDF level.

Also, $\gamma_{\min}$ is shown to be a monotonically decreasing function of the RMS EVM value of the EVM-optimized signals. Because the maximum power efficiency is inversely proportional to $\gamma_{\min}$ as shown in (34), $\rho_{\max}$ is increasing with RMS EVM thresholds. For $f = 12$, the upper bound of power efficiency is plotted for different RMS EVM thresholds in Fig. 3. The greater the target power efficiency is, the more the in-band distortion should be allowed.

Fig. 4 shows the achievable RMS EVM as a function of f for PAR thresholds γ =3, 4, 5, 6, and 7 dB. The tradeoff between RMS EVM and power efficiency can be improved if one is allowed to use more free subcarriers. The cost is the reduced bandwidth efficiency since fewer subcarriers are used for data transmission.

One realization of the EVM-optimized power allocation for $\mathbf{X}^{\dagger}$ is shown in Fig. 5. The PAR threshold was $\gamma = 3.95$ dB in this example. It shows that the optimized signal $\mathbf{X}^{\dagger}$ meets the spectral mask constraint imposed by the standards.

B. PAR Reduction Performance Comparison

Fig. 6 and Fig. 7 compare the PAR reduction performance of the proposed EVM optimization algorithm with several existing algorithms, including the repeated clipping and filtering (RCF) [25], iterative constrained clipping (ICC) [13] and PAR optimization algorithms [16].

In Fig. 6, the RMS EVM thresholds of these algorithms were all set to 0.1 so that they all satisfy the RMS EVM constraint. Specifically, this can be achieved by empirically predetermining the clipping threshold at 5.3 dB in the RCF algorithm. The ICC and PAR optimization algorithms both have a symbol-wise EVM constraint of 0.1. Also for the ICC algorithm, the clipping

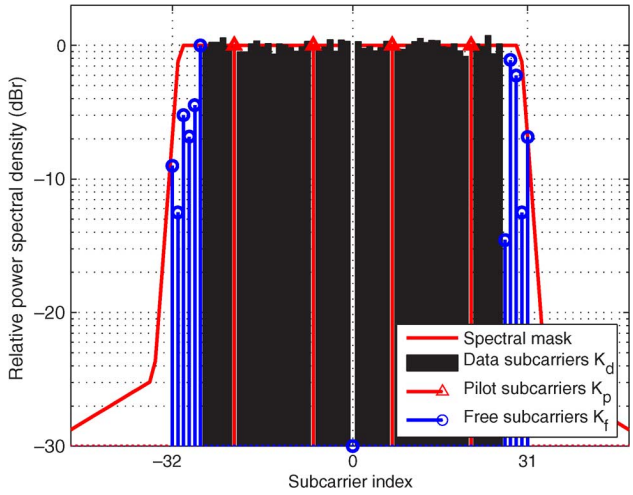

Fig. 5. One realization of the EVM-optimized power allocation for $\mathbf{X}^{\dagger}$; the PAR threshold is $\gamma = 3.95$ dB.

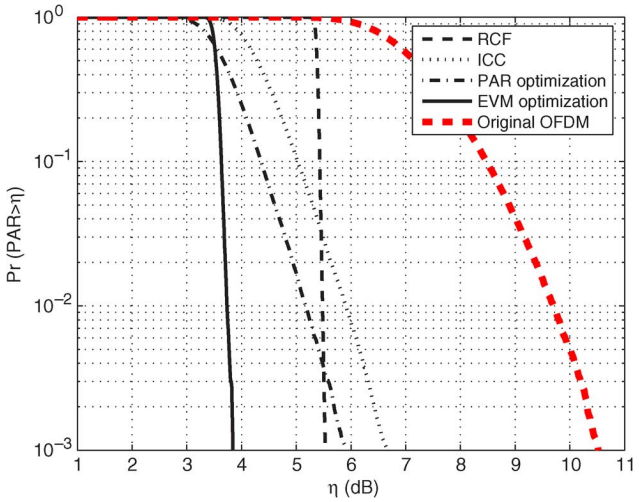

Fig. 6. CCDF curves of the PAR of the RCF, ICC, PAR optimization and EVM optimization algorithms, as well as the original OFDM signal; the number of free subcarriers is $f = 12$; the RMS EVM threshold 0.1 is satisfied by symbol-wise EVM constraint for ICC and PAR optimization, and by RMS EVM constraint for RCF and EVM optimization.

threshold of 2.8 dB was chosen so that the best PAR reduction performance can be obtained at the 10^{-3} CCDF level. Fifteen iterations were taken for RCF and ICC.

The EVM optimization algorithm is shown to have the best PAR reduction performance for the systems either with or without the symbol-wise linear scaling [18]. Without symbol-wise linear scaling, the power efficiency is inversely proportional to the maximum PAR. For the comparisons with RCF and ICC, as well as with the PAR optimization when no symbol-wise linear scaling is used, it is clear from Fig. 6 that the EVM optimization algorithm has a lower PAR (upper-bounded at a deterministic constraint of 3.95 dB) for almost all probabilities levels and thus, will have higher power efficiency. When the symbol-wise linear scaling is applied before the PA, on the other hand, the average power efficiency has been shown to be approximately inversely proportional to the harmonic mean of

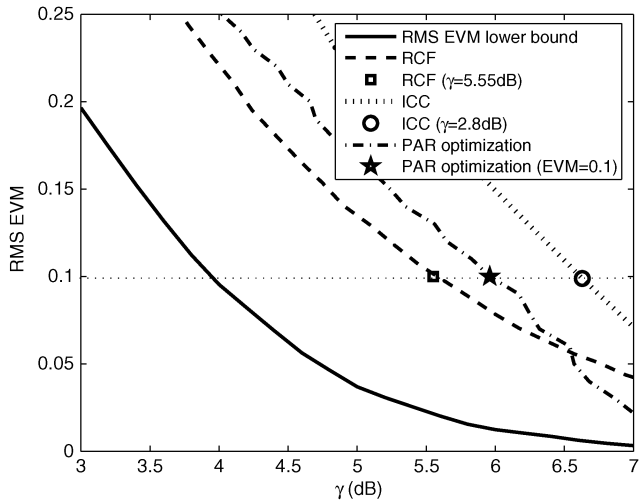

Fig. 7. γ-RMS EVM tradeoff curves of the RCF, ICC and PAR optimization methods, compared with the RMS EVM lower bound given by the EVM optimization algorithm; the number of free subcarriers is $f = 12$.

symbol-wise PAR [17, Eq. (18)]. Even though the CCDF curves of the EVM optimization and PAR optimization have a crossing point, it can be shown that the EVM optimization yields the smallest harmonic mean of symbol-wise PAR. As explained in Section I, the more precise allocation of the EVM allowance caused this improvement. When the PAR of an OFDM symbol is already less than the specified threshold, there is no advantage to further reduce it at the cost of distortion. Instead, allocating more EVM allowance to the symbols with greater PAR can result in a lower deterministic PAR threshold and thus better average PAR reduction performance.

Furthermore, the proposed EVM optimization is the only algorithm that guarantees the deterministic PAR constraint. The CCDF curves of ICC and PAR optimization methods have negative slopes. The clipped signals in the RCF method suffered from peak regrowth due to the filtering, which resulted in the PAR value of 5.55 dB at the 10^{-3} CCDF level although 5.3-dB clipping ratio was used. The peak regrowth will increase at lower CCDF levels. Thus, in order to show the γ-RMS EVM curves for these algorithms, the PAR value at the 10^{-3} CCDF level is over-optimistically chosen as the PAR threshold γ for the comparison algorithms. The exact γ-RMS EVM tradeoff can only be worse since 0.1% OFDM symbols are still saturated with $\mathrm{IBO} = \gamma$ for these algorithms.

For the same setup, the γ-RMS EVM tradeoff curves of the RCF, ICC, PAR optimization and EVM optimization algorithms are plotted in Fig. 7. The EVM optimization algorithm achieves the optimal tradeoff between RMS EVM and PAR threshold. It sets the lower bound for other algorithms. The tradeoff curves for the RCF and PAR optimization algorithms were obtained by varying the clipping ratio and the symbol-wise EVM threshold, respectively, but for the ICC algorithm, the clipping ratio was optimized for each symbol-wise EVM threshold offline so that the resulting PAR was minimized [13]. This provided the best tradeoff that could be achieved by the ICC algorithm. The specific examples shown in Fig. 6 (i.e., $\mathrm{RMS\ EVM} = 0.1$) confirm the tradeoff curves in Fig. 7.

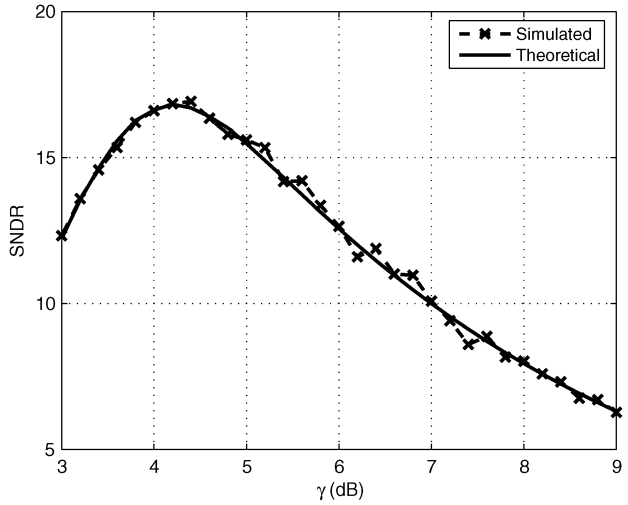

Fig. 8. SNDR versus PAR threshold γ curves of the Monte Carlo simulation and the SNDR approximation (39); PNR $= 20$ dB; the number of free subcarriers is $f = 12$.

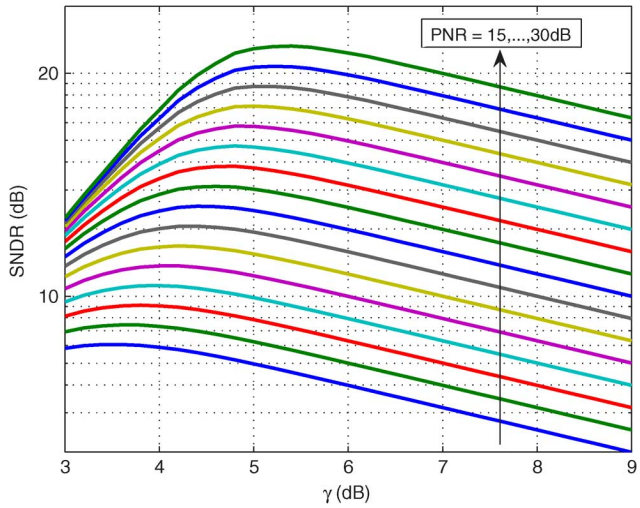

Fig. 9. SNDR as a function of the PAR threshold γ of EVM-optimized OFDM signal $\mathbf{x}^{\dagger}$ with PNR $= 15, 16, \cdots, 30$ dB (in step size of 1 dB), and the number of free subcarriers $f = 12$.

C. SNDR Maximization

Flat channels are assumed with additive white Gaussian channel noise where $h_k = h$ and $\sigma_k^2 = \sigma^2(\forall k)$ are assumed to be known at the transmitter.

First, define the PA-power-to-noise ratio (PNR) for the considered peak-power-limited class-A PA and channel as

$$\text{PNR} = \frac{rP|h|^2}{d \cdot \sigma^2} \tag{38}$$

which is completely determined by the transmitter setup and channel states. Thus, the SNDR expression in (30) is simplified as

$$\text{SNDR}_k \approx \frac{1 - (\text{RMS EVM})^2}{(\text{RMS EVM})^2 + \frac{2^{\gamma}}{\text{PNR}}}, \ \forall k \in \mathcal{K}_d. \tag{39}$$

For the given subcarrier setup, the RMS EVM value of the EVM-optimized signal is a function of the PAR threshold γ as shown in Fig. 2. Therefore, the optimal $\gamma^{\star}$ can be calculated for the given PNR value as discussed in Section III-C. Fig. 8 compares the SNDR versus PAR threshold γ curves obtained from Monte Carlo simulations with (29) and the SNDR approximation in (39). The approximate expression (39) is shown to be fairly accurate.

The approximation of (39) enables online parameter adjustment so that the maximum SNDR can be achieved when channel information is known. For PNR ranging from 15 to 30 dB, their SNDR curves are plotted in Fig. 9. They are calculated according to (39) and the γ-RMS EVM pairs obtained in Section IV-A. As expected, the greater the PNR, the greater the SNDR. Also, the optimal PAR threshold $\gamma^{\star}$ varies as a function of PNR. Fig. 10 summarizes the optimal $\gamma^{\star}$ and the corresponding RMS EVM values for PNR from 15 to 30 dB and $f = 12$. The main observation is, the greater the PNR, the larger the optimal PAR threshold $\gamma^{\star}$ and the smaller the optimal RMS EVM. Intuitively, when PNR is large, the channel noise has little effect and the distortion noise (i.e., RMS EVM) is dominant. Instead of trying to reduce the PAR threshold and

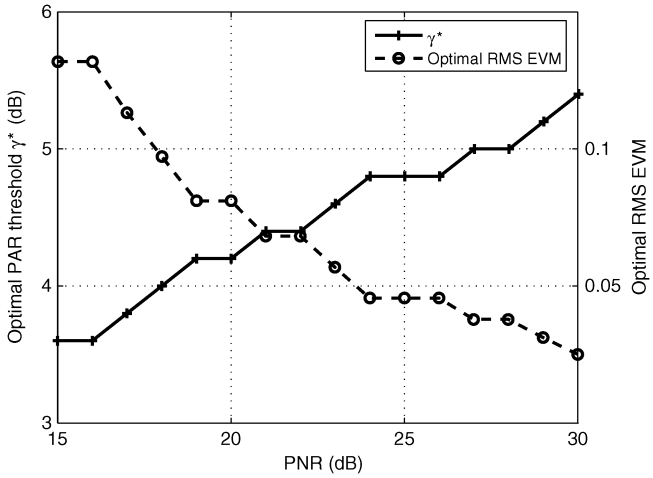

Fig. 10. SNDR-optimized PAR threshold $\gamma^{\star}$ and RMS EVM values for PNR $= 15, 16, \cdots, 30$ dB (in step size of 1 dB), and the number of free subcarriers $f = 12$.

increasing the average output power, lower level distortion should be pursued. On the other hand, when the channel noise is not negligible, reducing IBO by introducing nonlinear distortion can help to suppress the total noise and maximize SNDR. Moreover, the RMS EVM threshold ε given in the standard is not always optimal. For a small PNR, the optimal RMS EVM can be greater than ε.

D. Mutual Information Maximization

In [5] and [16], the idea of using "free subcarriers" or "reserved tones" to reduce PAR is presented. As is evident from Fig. 2, using free subcarriers facilitates PAR reduction. Here, in Fig. 11, we demonstrate how the mutual information lower bound varies with the number of free subcarriers. In this example the PNR value is set to 20 dB. The plot shows that the maximum mutual information lower bound is achieved at $(\gamma, f) = (5 \text{ dB}, 0)$ which means all subcarriers should be used for transmitting data and pilot signals, instead of being

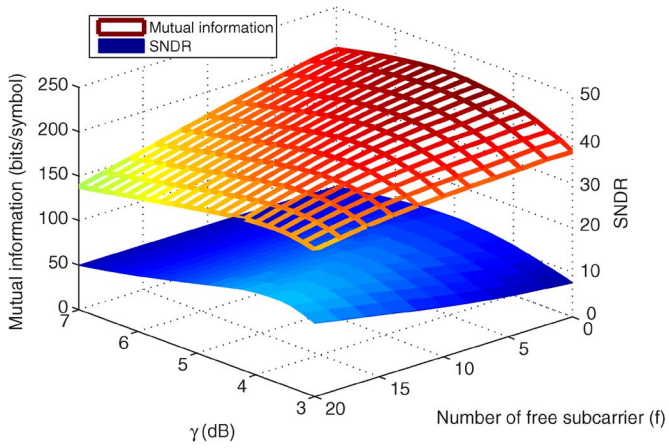

Fig. 11. Mutual information lower bounds and the corresponding SNDR values for the flat channel with PNR = 20 dB.

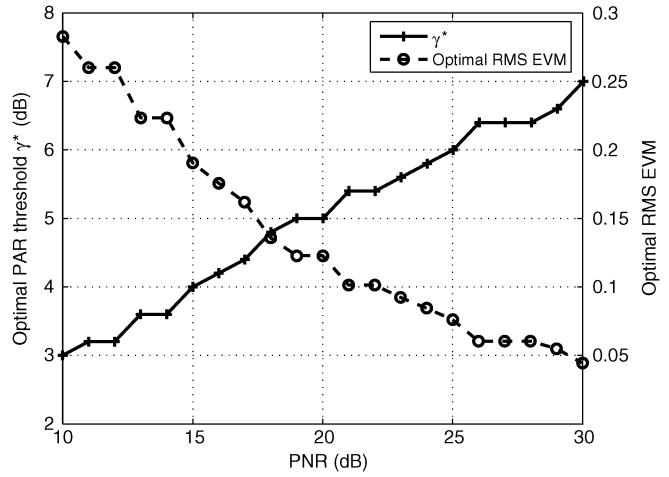

Fig. 12. Mutual information-optimized PAR threshold γ^* and RMS EVM values for PNR $= 10, 11, \cdots, 30$ dB; the optimal number of free subcarriers is always $f = 0$ by calculating the maximization problem of (37).

used to further reduce the distortion. On the contrary, the corresponding SNDR values will be maximized by using as many free subcarriers as possible. Different objectives yield different optimal system setups.

The optimal thresholds were calculated for different PNR values as shown in Fig. 12. Surprisingly, for the simulated PNR region, the optimal number of free subcarriers is always 0. Intuitively, the reason is that the symbol-wise EVM has already been minimized by the EVM optimization algorithm. With more free subcarriers, the help on further reducing the symbol-wise EVM is trivial. Instead, more subcarriers can be used for transmitting data so that the mutual information lower bound will be increased significantly.

This observation further simplifies the mutual information maximization problem. The number of free subcarriers can be prescribed to zero so that the mutual information maximization problem reduces to the SNDR maximization problem in Section III-C.

V. Conclusion

In this paper, we have developed a PAR reduction algorithm that guarantees a low fixed input back-off level and thus the signal will never be clipped by the PA. The proposed technique meets the spectral mask requirement and leads to a minimum symbol-wise EVM. We formulated a convex optimization problem which experiences no local minima and can be efficiently implemented by a customized interior-point method. The PAR threshold γ can be chosen such that the resulting RMS EVM value meets the standard's requirement. The maximum power efficiency can be reached by choosing the input back-off as the minimum PAR threshold $\gamma_{\min}$. The benefits of the proposed algorithm are reduced sensitivity to system nonlinearities and improved power efficiency. Also, the optimal tradeoffs between distortion, error rate, mutual information, and power efficiency have been investigated through extensive computer simulations.

Appendix A
Customized Interior-Point Method

To efficiently solve the symbol-wise EVM optimization problem in (12)–(18), the procedure of the iterative customized log-barrier interior-point method (IPM) is introduced in this appendix. The derivation can be referred to [26, ch. 11]. Because the standard IPM optimization technique can only deal with real numbers, the real-imaginary forms are used to represent complex matrices and vectors. In particular, the real-imaginary forms of an N-by-1 complex vector $\mathbf{X}$ and an m-by-n complex matrix $\mathbf{A}$ are, respectively,

$$\mathbb{X} = [\Re(X_0), \Im(X_0), \cdots, \Re(X_{N-1}), \Im(X_{N-1})]^T, \quad (40)$$

$$\mathbb{A} = \begin{bmatrix} \ddots & & \\ & \begin{matrix} \Re(A_{ij}) & -\Im(A_{ij}) \\ \Im(A_{ij}) & \Re(A_{ij}) \end{matrix} & \\ & & \ddots \end{bmatrix}_{2m \times 2n} \quad (41)$$

where $\Im(x)$ denotes the imaginary part of x.

The procedure of the customized IPM is

1) Initialize $\mathbf{X}^\dagger$ so that it satisfies all the constraints. For instance, in the IEEE 802.11a standard, $X_k^\dagger = 0$ $(k \in \mathcal{K}_f)$ satisfies the spectral mask constraint on free subcarriers; $X_1^\dagger = \sqrt{\sum_{k \in \mathcal{K}_d} |X_k|^2}$ and $X_k^\dagger = 0$ $(k \in \mathcal{K}_d$ but $k \neq 1)$ maintain the average power on data subcarriers not to be reduced; $X_k^\dagger = X_k$ $(k \in \mathcal{K}_p)$ keeps pilot subcarriers unchanged. The corresponding waveform $\mathbf{x}^\dagger$ has PAR close to 0 dB which satisfies practical deterministic PAR constraints. Also, initialize $e = 1.05\|\mathbf{S}(\mathbf{X} - \mathbf{X}^\dagger)\|_2$, obtained by backing off 5% from the EVM constraint (13). $\mathbf{S}$ is an $N \times N$ matrix indicating the locations of the data subcarriers, whose (m, n)th element is given by

$$S_{m,n} = \begin{cases} 1, & m = n \in \mathcal{K}_d \\ 0, & m \notin \mathcal{K}_d, \text{ or } n \notin \mathcal{K}_d, \text{ or } m \neq n. \end{cases} \quad (42)$$

Thus, $\mathbf{S}$ consists of block identity and zero matrices, and the symbol-wise EVM in (9) can be rewritten as $\epsilon(\mathbf{X}, \mathbf{X}^\dagger) = (1/\sqrt{dP_0})\|\mathbf{S}(\mathbf{X} - \mathbf{X}^\dagger)\|_2$.

2) Update the following variables:

$$\delta_a = \frac{e^2}{2} + \Re\left(\mathbf{X}^H \mathbf{S}(\mathbf{X}^\dagger - \mathbf{X})\right) \tag{43}$$

$$\delta_e = e^2 - \left\|\mathbf{S}(\mathbf{X} - \mathbf{X}^\dagger)\right\|_2^2 \tag{44}$$

$$\delta_n = \gamma\sigma_x^2 - \left|x^\dagger[n]\right|^2,\ n \in \{0, \cdots, LN-1\} \tag{45}$$

$$\phi_k = \begin{cases} \mathcal{M}_k \cdot P_0 - \left|X_k^\dagger\right|^2, & k \in \mathcal{K}_f, \\ 0, & \text{otherwise} \end{cases} \tag{46}$$

where γ is the PAR upper bound in (11). All these variables should remain positive as required by the inequality constraints.

3) Calculate the gradient vector $\mathbb{G}$ according to

$$\mathbb{G} = \frac{4e}{\delta_e^2}\mathbb{S}(\mathbb{X}^\dagger - \mathbb{X}) - \frac{e}{\delta_a^2}\mathbb{S}\mathbb{X} \tag{47}$$

where $\mathbb{S}$, $\mathbb{X}$ and $\mathbb{X}^\dagger$ are the real-imaginary forms of $\mathbf{S}$, $\mathbf{X}$ and $\mathbf{X}^\dagger$, respectively.

4) Calculate the Hessian matrix $\mathbb{H}$ according to

$$\mathbb{H} = -(\mathbb{A} + \mathbb{E} + \mathbb{M} + \mathbb{Q}^T\mathbb{P}\mathbb{Q}) \tag{48}$$

where

$$\mathbb{A} = -\frac{1}{\delta_a^2}(\mathbb{S}\mathbb{X})(\mathbb{S}\mathbb{X})^T \tag{49}$$

$$\mathbb{E} = -\frac{2}{\delta_e}\mathbb{S} - \frac{4}{\delta_e^2}\mathbb{S}(\mathbb{X}^\dagger - \mathbb{X})(\mathbb{X}^\dagger - \mathbb{X})^T\mathbb{S}^T \tag{50}$$

$$\mathbb{M} = \text{blkdiag}(\mathbb{M}_0, \cdots, \mathbb{M}_{N-1}) \tag{51}$$

$$\mathbb{P} = \text{blkdiag}(\mathbb{P}_0, \cdots, \mathbb{P}_{LN-1}) \tag{52}$$

with blkdiag() denoting the block-diagonal structure and $\mathbb{M}_k \in \mathcal{R}^{2\times 2}$ being

$$\mathbb{M}_k = \frac{2}{\phi_k^2}\begin{bmatrix} -\phi_k - 2\left(\Re\left(X_k^\dagger\right)\right)^2 & -2\Re\left(X_k^\dagger\right)\Im\left(X_k^\dagger\right) \\ -2\Re\left(X_k^\dagger\right)\Im\left(X_k^\dagger\right) & -\phi_k - 2\left(\Im\left(X_k^\dagger\right)\right)^2 \end{bmatrix} \tag{53}$$

for $k \in \mathcal{K}_f$, and $\mathbb{M}_k = \mathbf{0}_{2\times 2}$, otherwise. Matrix $\mathbb{P}_n \in \mathcal{R}^{2\times 2}(n \in \{0, \cdots, LN-1\})$ is

$$\mathbb{P}_n = \frac{2}{\delta_n^2}\begin{bmatrix} -\delta_n - 2\left(\Re\left(x^\dagger[n]\right)\right)^2 & -2\Re\left(x^\dagger[n]\right)\Im\left(x^\dagger[n]\right) \\ -2\Re\left(x^\dagger[n]\right)\Im\left(x^\dagger[n]\right) & -\delta_n - 2\left(\Im\left(x^\dagger[n]\right)\right)^2 \end{bmatrix}.$$

Moreover, if $\mathbf{F}$ is the L-times oversampling IFFT matrix such that $\mathbf{x}^\dagger = \mathbf{F}\mathbf{X}^\dagger$, $\mathbf{Q}$ consists of the corresponding $d+f$ columns of $\mathbf{F}$ with the column indices in $\mathcal{K}_d \bigcup \mathcal{K}_f$, and $\mathbb{Q}$ is the real-imaginary form of $\mathbf{Q}$.

The computation of (48) is mainly consisted of the matrix multiplication $\mathbb{Q}^T\mathbb{P}\mathbb{Q}$. By using the diagonalization properties of FFT, the complexity of constructing the Hessian matrix $\mathbb{H}$ can be reduced in the similar way as shown in [16].

5) Solve the updating vector $\mathbb{V}$ in

$$\mathbb{H}\mathbb{V} = -\mathbb{G}. \tag{54}$$

Numerical methods, e.g. Cholesky factorization and conjugate gradient methods, can be used. The complex form $\mathbf{V}$ of $\mathbb{V}$ can be found by (40). And the time-domain updating vector has $\mathbf{v} = [v[0], \cdots, v[LN-1]]^T = \text{IFFT}_L(\mathbf{V})$.

6) Determine the step size β according to

$$\beta = \xi \min\{\beta_a, \beta_e, \beta_n, \hat{\beta}_k, e\},\ \text{for } n \in \{0, \cdots, LN-1\},\ k \in \mathcal{K}_f \tag{55}$$

where ξ is selected as a positive number less than 1 to ensure the updated point remain strictly feasible. Here, $\xi = 0.95$ is empirically chosen for fast convergence speed. $\beta_a, \beta_e, \beta_n (n \in \{0, \cdots, LN-1\})$ and $\hat{\beta}_k (k \in \mathcal{K}_f)$ are determined by the average power constraint (16), EVM minimization (13), peak power constraint (18) and free subcarrier spectral mask (15), respectively. The results are: β_a is

$$b_a = \Re(\mathbf{X}^H\mathbf{S}\mathbf{V}) - e,$$

$$\beta_a = \begin{cases} -b_a - \sqrt{b_a^2 - 2\delta_a}, & b_a < 0 \text{ and } b_a^2 - 2\delta_a \geq 0 \\ \infty, & \text{otherwise.} \end{cases}$$

β_e is

$$a_e = \|\mathbf{V}\|_2^2 - 1$$

$$b_e = e + \Re\left((\mathbf{X}^\dagger - \mathbf{X})^H\mathbf{S}\mathbf{V}\right)$$

$$\beta_e = \begin{cases} \frac{-b_e + \sqrt{b_e^2 + a_e\delta_e}}{a_e}, & a_e > 0 \text{ or } (a_e < 0 \text{ and } b_e > 0) \\ \frac{\delta_e}{2b_e}, & a_e = 0 \text{ and } b_e > 0 \\ \infty, & \text{otherwise.} \end{cases}$$

$\beta_n (n \in \{0, \cdots, LN-1\})$ has

$$a_n = |v[n]|^2$$

$$b_n = \Re\left(\left(x^\dagger[n]\right)^* v[n]\right)$$

$$\beta_n = \begin{cases} \frac{-b_n + \sqrt{b_n^2 + a_n\delta_n}}{a_n}, & a_n \neq 0 \\ \frac{\delta_n}{2b_n}, & a_n = 0 \text{ and } b_n > 0 \\ \infty, & \text{otherwise.} \end{cases}$$

And $\hat{\beta}_k (k \in \mathcal{K}_f)$ has

$$\hat{a}_k = |V_k|^2,$$

$$\hat{b}_k = \Re\left(X_k^{\dagger *} V_k\right)$$

$$\hat{\beta}_k = \begin{cases} \frac{-\hat{b}_k + \sqrt{\hat{b}_k^2 + \hat{a}_k\phi_k}}{\hat{a}_k}, & \hat{a}_k \neq 0 \\ \frac{\phi_k}{2\hat{b}_k}, & \hat{a}_k = 0 \text{ and } \hat{b}_k > 0 \\ \infty, & \text{otherwise.} \end{cases}$$

7) Update $\mathbf{X}^\dagger$ and e according to

$$\mathbf{X}_{\text{new}}^\dagger = \mathbf{X}^\dagger + \beta\mathbf{V} \tag{56}$$

$$e_{\text{new}} = e - \beta. \tag{57}$$

8) Stop if the algorithm converges or the maximum number of iterations has been reached, or return to Step 2 and start a new iteration.

Good convergence can generally be found within ten iterations, for which the difference between the solution EVM and the optimal EVM is less than 0.001.

Appendix B
SNDR Approximation

For the peak-power-limited transmitter with a class-A PA, we assume that the total power consumed by the PA for transmitting one OFDM symbol is constant and denoted as P, which has

$$P = 2LN(\mathcal{G}\mu_{\text{in}})^2. \tag{58}$$

In order to derive the SNDR, the power transmitted on data subcarriers and the attenuation factor α should be analyzed. Since there is not a closed form expression linking $\mathbf{X}$ to $\mathbf{X}^\dagger$, it is difficult to analyze the data subcarrier power and α theoretically. However, we can use some simplifying assumptions to approximate the SNDR.

We assume the error vector $\mathbf{X} - \mathbf{X}^\dagger$ is uncorrelated with the data vector $\mathbf{X}$ and the equality of (21) holds, i.e.,

$$E\left[\sum_{k\in\mathcal{K}_d}\left|X_k^\dagger\right|^2\right] \approx E\left[\sum_{k\in\mathcal{K}_d}|X_k|^2\right]. \tag{59}$$

This approximation is quite accurate because the difference between $\mathbf{X}$ and $\mathbf{X}^\dagger$ is small as shown to in Section IV. Thus, the actually transmitted power on the data subcarriers can be approximated by

$$\mathcal{G}^2\mathcal{B}^2E\left[\sum_{k\in\mathcal{K}_d}\left|X_k^\dagger\right|^2\right] \approx \mathcal{G}^2\mathcal{B}^2rLN\sigma_x^2 \tag{60}$$

where r is defined in (31). By substituting $\mathcal{B} = \sqrt{\mu_{\text{in}}^2/\sigma_x^2\text{IBO}}$ and (58) into (60), we simplify (60) to

$$\mathcal{G}^2\mathcal{B}^2E\left[\sum_{k\in\mathcal{K}_d}\left|X_k^\dagger\right|^2\right] \approx \frac{rP}{2\text{IBO}} \tag{61}$$

and the average transmitted power of each data subcarrier is denoted as

$$P_{\text{d}} = \frac{rP}{2d\text{IBO}}. \tag{62}$$

Next, when the RMS EVM is not large, the average distortion power can be approximated as

$$\mathcal{G}^2\mathcal{B}^2\sigma_\omega^2 \approx \mathcal{G}^2\mathcal{B}^2E\left[\left|X_k^\dagger - X_k\right|^2\right] \tag{63}$$

$$= (\text{RMS EVM})^2P_{\text{d}} \tag{64}$$

so that the signal power is $|\alpha|^2P_{\text{d}} \approx (1-(\text{RMS EVM})^2)P_{\text{d}}$.

Therefore, (29) becomes

$$\text{SNDR}_k \approx \frac{|h_k|^2\left(1-(\text{RMS EVM})^2\right)P_{\text{d}}}{|h_k|^2(\text{RMS EVM})^2P_{\text{d}}+\sigma_k^2}, \quad (k\in\mathcal{K}_d). \tag{65}$$

Substituting (62) into (65) and setting $\text{IBO} = \gamma$ which maximizes the power efficiency, the SNDR expression in (30) follows in the end. The above approximations were shown to yield good accuracy in Section IV-C by the comparison with simulation results.

References

[1] *EN300744: Digital Video Broadcasting (DVB): Framing Structure, Channel Coding and Modulation for Digital Terrestrial Television*, EN300744, Eur. Telecommun. Standards Inst. (ETSI), 1997, Sophia Antipolis, France.

[2] *Wireless LAN Medium Access Control (MAC) and Physical Layer (PHY) Specifications: High-Speed Physical Layer in the 5 GHz Band*, IEEE Std. 802.11a, Sep. 1999.

[3] *IEEE Standard for Local and Metropolitan Area Networks Part 16: Air Interface for Fixed Broadband Wireless Access Systems*, IEEE Std. 802.16-2004, 2004, (Revision of IEEE Std. 802.16-2001).

[4] S. H. Han and J. H. Lee, "An overview of peak-to-average power ratio reduction techniques for multicarrier transmission," *IEEE Wireless Commun. Mag.*, vol. 12, no. 2, pp. 56–65, Apr. 2005.

[5] J. Tellado, *Multicarrier Modulation With Low PAR: Applications to DSL and Wireless*. Norwell, MA: Kluwer, Sep. 2000.

[6] R. W. Bauml, R. F. H. Fischer, and J. B. Huber, "Reducing the peak-to-average power ratio of multicarrier modulationby selected mapping," *Electron. Lett.*, vol. 32, no. 22, pp. 2056–2057, Oct. 1996.

[7] S. H. Muller and J. B. Huber, "OFDM with reduced peak-to-average power ratio by optimum combination of partial transmit sequences," *Electron. Lett.*, vol. 33, no. 5, pp. 368–369, Feb. 1997.

[8] D. Kim and G. L. Stüber, "Clipping noise mitigation for OFDM by decision-aided reconstruction," *IEEE Commun. Lett.*, vol. 3, no. 1, pp. 4–6, Jan. 1999.

[9] R. J. Baxley, "Analyzing selected mapping for peak-to-average power reduction in OFDM," M.S. thesis, Georgia Inst. of Technology, Atlanta, Jun. 2005.

[10] T. Jiang and Y. Wu, "An overview: Peak-to-average power ratio reduction techniques for OFDM signals," *IEEE Trans. Broadcast.*, vol. 54, no. 2, pp. 257–268, Jun. 2008.

[11] H. Ochiai and H. Imai, "Performance analysis of deliberately clipped OFDM signals," *IEEE Trans. Commun.*, vol. 50, no. 1, pp. 89–101, Jan. 2002.

[12] B. S. Krongold and D. L. Jones, "PAR reduction in OFDM via active constellation extension," *IEEE Trans. Broadcast.*, vol. 49, no. 3, pp. 258–268, Sep. 2003.

[13] R. J. Baxley, C. Zhao, and G. T. Zhou, "Constrained clipping for crest factor reduction in OFDM," *IEEE Trans. Broadcast.*, vol. 52, no. 4, pp. 570–575, Dec. 2006.

[14] B. S. Krongold and D. L. Jones, "An active-set approach for OFDM PAR reduction via tone reservation," *IEEE Trans. Signal Process.*, vol. 52, no. 2, pp. 495–509, Feb. 2004.

[15] E. Lawrey and C. J. Kikkert, "Peak to average power ratio reduction of OFDM signals using peak reduction carriers," in *Proc. ISSPA*, Brisbane, QLD, Australia, Aug. 1999, vol. 2, pp. 737–740.

[16] A. Aggarwal and T. H. Meng, "Minimizing the peak-to-average power ratio of OFDM signals using convex optimization," *IEEE Trans. Signal Process.*, vol. 54, no. 8, pp. 3099–3110, Aug. 2006.

[17] Q. Liu, R. J. Baxley, and G. T. Zhou, "Free subcarrier optimization for peak-to-average power ratio minimization in OFDM systems," in *Proc. IEEE ICASSP*, Las Vegas, NV, Mar. 2008, pp. 3073–3076.

[18] H. Ochiai, "Performance analysis of peak power and band-limited OFDM system with linear scaling," *IEEE Trans. Wireless Commun.*, vol. 2, no. 5, pp. 1055–1065, Sep. 2003.

[19] E. Costa, M. Midrio, and S. Pupolin, "Impact of amplifier nonlinearities on OFDM transmission system performance," *IEEE Commun. Lett.*, vol. 3, no. 2, pp. 37–39, Feb. 1999.

[20] A. N. D'Andrea, V. Lottici, and R. Reggiannini, "RF power amplifier linearization through amplitude and phase predistortion," *IEEE Trans. Commun.*, vol. 44, no. 11, pp. 1477–1484, Nov. 1996.

[21] S. Andreoli, H. G. McClure, P. Banelli, and S. Cacopardi, "Digital linearizer for RF amplifiers," *IEEE Trans. Broadcast.*, vol. 43, no. 1, pp. 12–19, Mar. 1997.

[22] C. Zhao, R. J. Baxley, and G. T. Zhou, "Peak-to-average power ratio and power efficiency considerations in MIMO-OFDM systems," *IEEE Commun. Lett.*, vol. 12, no. 4, pp. 268–270, Apr. 2008.

[23] R. Raich, H. Qian, and G. T. Zhou, "Optimization of SNDR for amplitude-limited nonlinearities," *IEEE Trans. Commun.*, vol. 53, no. 11, pp. 1964–1972, Nov. 2005.

[24] H. E. Rowe, "Memoryless nonlinearities with Gaussian inputs: Elementary results," *Bell Syst. Tech. J.*, vol. 61, pp. 1519–1525, Sep. 1982.
[25] J. Armstrong, "Peak-to-average power reduction for OFDM by repeated clipping and frequency domain filtering," *Electron. Lett.*, vol. 38, pp. 246–247, Feb. 2002.
[26] S. Boyd and L. Vandenberghe, *Convex Optimization*. Cambridge, U.K.: Cambridge Univ. Press, Mar. 2004.

Qijia Liu (S'05) received the B.E. and M.S. degrees in electrical engineering from Tsinghua University, Beijing, China, in 2004 and 2007, respectively. He is currently working toward the Ph.D. degree in electrical engineering at the Georgia Institute of Technology, Atlanta.

His research interests include multicarrier communications theory, signal processing, and optimizations.

Robert J. Baxley (S'02–M'08) received the B.S., M.S., and Ph.D. degrees, all in electrical engineering, from the Georgia Institute of Technology (Georgia Tech), Atlanta, in 2003, 2005, and 2008, respectively.

He is a Research Engineer with the Georgia Tech Research Institute (GTRI) Information Technology and Telecommunications Lab (ITTL). His current research interests include communications theory, signal processing, and statistics.

Dr. Baxley received the institute-wide Sigma Xi award for best M.S. thesis in 2005, and he is a recipient of the National Science Foundation Graduate Research Fellowship.

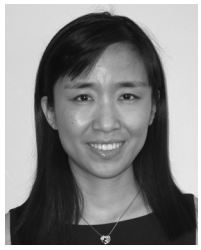

Xiaoli Ma (SM'09) received the B.S. degree in automatic control from Tsinghua University, Beijing, China, in 1998, the M.S. degree in electrical engineering from the University of Virginia, Charlottesville, in 2000, and the Ph.D. degree in electrical engineering from the University of Minnesota, Minneapolis, in 2003.

From 2003 to 2005, she was an Assistant Professor of electrical and computer engineering at Auburn University, Auburn, AL. Since 2006, she has been with the School of Electrical and Computer Engineering, Georgia Institute of Technology, Atlanta. Her research interests include transceiver designs for wireless fading channels, channel modeling, estimation and equalization, synchronization for OFDM systems, and routing and cooperative designs for wireless networks.

Dr. Ma serves as an Associate Editor for the IEEE SIGNAL PROCESSING LETTERS and the IEEE TRANSACTIONS ON WIRELESS COMMUNICATIONS.

G. Tong Zhou (SM'00) received the B.Sc. degree in biomedical engineering and instrumentation from Tianjin University, Tianjin, China, in 1989 and the M.Sc. degree in biophysics, the M.Sc. degree in electrical engineering, and the Ph.D. degree in electrical engineering, all from the University of Virginia (UVA), Charlottesville, in 1992, 1993, and 1995, respectively.

Since September 1995, she has been with the School of Electrical and Computer Engineering, Georgia Institute of Technology, Atlanta, where she is now a Professor. Her research interests are in the general areas of statistical signal processing and communications applications.

Dr. Zhou received the National Science Foundation Faculty Early Career Development (CAREER) Award in 1997. She served as Chair of the IEEE Signal Processing Society Signal Processing Theory and Methods Technical Committee during 2006 and 2007.